Coherent Detection of Frequency-Hopped Quadrature Modulations in the Presence of Jamming—Part I: QPSK and QASK Modulations

MARVIN K. SIMON, FELLOW, IEEE, AND ANDREAS POLYDOROS

Abstract—**This paper examines the performance of coherent QPSK and QASK systems combined with FH or FH/PN spread spectrum techniques in the presence of partial-band multitone or noise jamming. The worst-case jammer and worst-case performance are determined as functions of the signal-to-background noise ratio (SNR) and signal-to-jammer power ratio (SJR). Asymptotic results for high SNR are shown to have a linear dependence between the jammer's optimal power allocation and the system error probability performance.**

I. INTRODUCTION

QUADRIPHASE shift keying (QPSK), quadrature amplitude shift keying (QASK), and quadrature partial response (QPR)[1] are bandwidth-efficient modulation techniques whose performance over the additive "white" Gaussian noise channel is well documented in the literature [1]-[3]. The purpose of this paper is to present the comparable results when a frequency-hopping (FH) spread spectrum modulation is superimposed on these conventional techniques in order to combat the intentional interference introduced by a jammer.

In general, two possibilities exist with regard to the manner in which the FH modulation is implemented. If the individual hop pulse phases bear no relation to each another, the spread spectrum technique is referred to as *noncoherent FH*. If, on the other hand, phase continuity is maintained from one hop pulse to another, *coherent FH* is obtained. In either case, one usually makes the assumption that the hop pulse phase is constant over a single hop interval. In this paper, we shall consider the coherent FH case only; thus, the receiver structures analyzed will be those normally employed for coherent detection of QPSK and QASK in an additive white Gaussian noise background.

Pseudonoise (PN) direct-sequence balanced modulation of the individual FH frequencies may also be employed to improve the ability to combat jamming interference. This hybrid technique is simply known as FH/PN modulation. In this paper, we shall also consider the antijam capabilities of FH/PN-QPSK and FH/PN-QASK.

In designing any spread spectrum system to be jam-resistant, one must propose a scenario under which the jammer is assumed to operate. As such, one normally assumes an intelligent jammer in that he has knowledge of the form of data and spread spectrum modulations, including such items as data rate, spreading bandwidth, and hop rate, but no knowledge of the code selected for determining the spectrum-spreading hop frequencies. Thus, the strategy normally employed is to design for the worst case in the sense that, given the modulation form of the communicator, the jammer is assumed to employ the type of jamming which is most deleterious to the communication receiver.

While many possible jammer models can be proposed, the most common are partial-band (PB) noise jamming and partial-band multitone jamming. In this paper, we shall treat these two jamming types separately and develop, in each case, the performance corresponding to a worst-case jammer strategy.

Part I of the paper will examine the performance of coherent QPSK and QASK systems combined with FH or FH/PN spread spectrum techniques in the presence of PB multitone or noise jamming. The worst-case jammer and worst-case performance will be determined as functions of the signal-to-background noise ratio (SNR) and signal-to-jammer power ratio (SJR). Asymptotic results for high SNR will be shown to have a linear dependence between the jammer's optimal power allocation and the system error probability performance.

Part II of the paper [8] will consider the performance of QPR in the presence of the identical jamming postulated in Part I. Although a QPR system employs a single sample detector in its receiver, while QASK (or QPSK) requires a matched filter type of receiver, it will be shown that the coherent detection performances of the two in the presence of the intentional jammer have definite similarities.

Before leaving the Introduction, we point out that the assumption of coherent FH bears with it the assumption that the coherent synthesizer in the receiver is required to estimate and correct for the phase errors associated with the electrical path length over the channel and, more importantly, the Doppler shift which, with frequency hopping, is a function of frequency. A discussion of techniques for accomplishing this important and difficult task is beyond the scope of this paper other than to mention the fact that state-of-the-art coherent frequency synthesizers will undoubtedly allow the design of such a system to be feasible in the near future.

Paper approved by the Editor for Communication Theory of the IEEE Communications Society for publication after presentation at the International Telemetering Conference, San Diego, CA, 1980. Manuscript received September 17, 1980; revised March 5, 1981. This work was performed by M. K. Simon as a Consultant to Axiomatix, Los Angeles, CA.

M. K. Simon is with the Jet Propulsion Laboratory, Pasadena, CA 91103.

A. Polydoros is with Axiomatix, Los Angeles, CA 90045.

[1] The QPR Class I modulation is also referred to in the literature as duobinary encoded QPSK [1].

0090-6778/81/1100-1644$00.75

II. PERFORMANCE OF FH-QPSK IN THE PRESENCE OF PARTIAL-BAND MULTITONE JAMMING

An FH-QPSK signal is characterized by transmitting (Fig. 1)

$$s^{(i)}(t) = \sqrt{2S}\sin(\omega_H{}^{(i)}t + \theta^{(i)}) \tag{1}$$

in the ith signaling interval $(i-1)T_s \leqslant t \leqslant iT_s$, where $\omega_H{}^{(i)}$ is the particular carrier frequency selected by the frequency hopper for this interval.[2] According to the designated spread spectrum code, $\theta^{(i)}$ is the information symbol which ranges over the set of possible values

$$\theta_m = \frac{m\pi}{4}; \qquad m = 1, 3, 5, 7 \tag{2}$$

and S is the transmitted average power.

At the receiver (Fig. 2), the sum of additive white Gaussian noise $n(t)$, the jammer $j(t)$, and a random phase-shifted version of the transmitted signal $s(t;\theta)$ are first frequency dehopped, then coherently demodulated by a conventional QPSK demodulator.

The bandpass noise $n(t)$ has the usual narrow-band representation

$$n(t) = \sqrt{2}[N_c(t)\cos(\omega_H{}^{(i)}t + \theta) - N_s(t)\sin(\omega_H{}^{(i)}t + \theta)] \tag{3}$$

where $N_c(t)$ and $N_s(t)$ are statistically independent low-pass white Gaussian noise processes with single-sided noise spectral density N_0 W/Hz. The PB multitone jammer $j(t)$ is assumed to have a total power J which is evenly divided among q jammer tones. Thus, each tone has power

$$J_0 = \frac{J}{q}. \tag{4}$$

Furthermore, since the jammer is assumed to have knowledge of the hop frequencies or, equivalently, the exact location of the spreading bandwidth W and the number N of hops in this bandwidth, it is safe to assume that he will randomly locate each of his q tones coincident with q of the N hop frequencies. Thus,

$$\alpha \triangleq \frac{q}{N} \tag{5}$$

represents the fraction of the total band which is continuously jammed with tones, each having power J_0. Once again, the jammer's strategy is to distribute his total power J (i.e., choose α and J_0) in such a way as to cause the communicator to have maximum probability of error.

[2] We assume for simplicity that the hop rate is equal to or a submultiple of the information symbol rate and that the frequency hopper and symbol clock are synchronous. Thus, in a given symbol interval, the signal frequency is constant and the jammer, if transmitting a tone at that frequency, affects the entire symbol interval.

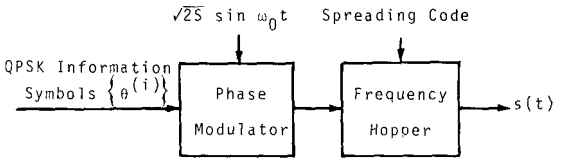

Fig. 1. Block diagram of an FH-QPSK modulator.

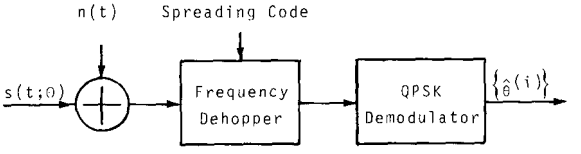

Fig. 2. Block diagram of an FH-QPSK demodulator.

In view of the foregoing, the total received signal in a signaling interval which contains a jamming tone at the hop frequency is given by

$$y^{(i)}(t) = s^{(i)}(t;\theta) + n(t) + j(t) \tag{6}$$

where

$$s^{(i)}(t;\theta) = \sqrt{2S}\sin(\omega_H{}^{(i)}t + \theta^{(i)} + \theta). \tag{7}$$

$n(t)$ is given by (3) and

$$j(t) = \sqrt{2J_0}\cos(\omega_H{}^{(i)}t + \theta_j + \theta) \tag{8}$$

with θ_j uniformly distributed on $(0, 2\pi)$ and independent of the information symbol phase $\theta^{(i)}$. Over an integral number of hop bands, the fraction α of the total number of signaling intervals will be characterized by (6). In the remaining fraction $(1-\alpha)$ of the signaling intervals, the received signal is simply characterized by

$$y^{(i)}(t) = s^{(i)}(t;\theta) + n(t). \tag{9}$$

After ideal coherent demodulation by the frequency hopper, the in-phase and quadrature components of the received signal become[3]

$$\begin{aligned}\epsilon_I(t) &\triangleq y^{(i)}(t)[\sqrt{2}\sin(\omega_H{}^{(i)}t + \theta)] \\ &= \sqrt{S}\cos\theta^{(i)} - \sqrt{J_0}\sin\theta_j - N_s(t) \\ \epsilon_Q(t) &\triangleq y^{(i)}(t)[\sqrt{2}\cos(\omega_H{}^{(i)}t + \theta)] \\ &= \sqrt{S}\sin\theta^{(i)} + \sqrt{J_0}\cos\theta_j + N_c(t).\end{aligned} \tag{10}$$

These signals are then passed through integrate-and-dump filters of duration equal to the information symbol interval

[3] We ignore double-harmonic terms.

T_s to produce the in-phase and quadrature decision variables

$$\begin{aligned} z_I &\triangleq \int_{(i-1)T_s}^{iT_s} \epsilon_I(t)\,dt \\ &= \sqrt{S}\,T_s \cos\theta^{(i)} - \sqrt{J_0}\,T_s \sin\theta_j + N_I \\ &= a_i \sqrt{\frac{S}{2}}\,T_s - \sqrt{J_0}\,T_s \sin\theta_j + N_I \\ z_Q &\triangleq \int_{(i-1)T_s}^{iT_s} \epsilon_Q(t)\,dt \\ &= \sqrt{S}\,T_s \sin\theta^{(i)} + \sqrt{J_0}\,T_s \cos\theta_j + N_Q \\ &= b_i \sqrt{\frac{S}{2}}\,T_s + \sqrt{J_0}\,T_s \cos\theta_j + N_Q \end{aligned} \tag{11}$$

where

$$\begin{aligned} N_I &\triangleq -\int_{(i-1)T_s}^{iT_s} N_s(t)\,dt \\ N_Q &\triangleq \int_{(i-1)T_s}^{iT_s} N_c(t)\,dt \end{aligned} \tag{12}$$

are zero-mean Gaussian random variables with variance $N_0 T_s/2$ and, in view of the possible values for $\theta^{(i)}$ given in (2), $\{a_i\}$ and $\{b_i\}$ are the equivalent independent in-phase and quadrature binary information sequences which take on values ± 1.

The receiver estimates of a_i and b_i are obtained by passing z_I and z_Q through hard limiters, giving

$$\hat{a}_i = \operatorname{sgn} z_I; \quad \hat{b}_i = \operatorname{sgn} z_Q. \tag{13}$$

Hence, given a_i, b_i, and θ_j, the probability that the ith symbol is in error is the probability that either $\hat{a}_i$ *or* $\hat{b}_i$ is in error, i.e.,

$$\begin{aligned} P_{E_i}(\theta_j) &= \text{Prob}\,\{\hat{a}_i \neq a_i \text{ or } \hat{b}_i \neq b_i\} \\ &= \text{Prob}\,\{\hat{a}_i \neq a_i\} + \text{Prob}\,\{\hat{b}_i \neq b_i\} \\ &\quad - \text{Prob}\,\{\hat{a}_i \neq a_i\}\,\text{Prob}\,\{\hat{b}_i \neq b_i\}. \end{aligned} \tag{14}$$

Since the signal set is symmetric, we can compute (14) for any of the four possible signal points and obtain the average probability of symbol error conditioned on the jammer phase $\bar{P}_E(\theta_j)$. Thus, assuming for simplicity that $a_i = 1$, $b_i = 1$, we compute $\bar{P}_E(\theta_j)$ from (14), combined with (11) and (13), as

$$\begin{aligned} \bar{P}_E(\theta_j) &= \text{Prob}\,\{z_I < 0 \mid a_i = 1\} + \text{Prob}\,\{z_Q < 0 \mid b_i = 1\} \\ &\quad - \text{Prob}\,\{z_I < 0 \mid a_i = 1\}\,\text{Prob}\,\{z_Q < 0 \mid b_i = 1\} \\ &= P_s(\theta_j) + P_c(\theta_j) - P_s(\theta_j) P_c(\theta_j) \end{aligned} \tag{15}$$

where[4]

$$\begin{aligned} P_s(\theta_j) &= \text{Prob}\left\{N_I < -\sqrt{\frac{S}{2}}\,T_s + \sqrt{J_0}\,T_s \sin\theta_j\right\} \\ &= Q\left[\sqrt{\frac{ST_s}{N_0}}\left(1 - \sqrt{\frac{2J_0}{S}}\,\sin\theta_j\right)\right] \\ P_c(\theta_j) &= \text{Prob}\left\{N_Q < -\sqrt{\frac{S}{2}}T_s - \sqrt{J_0}T_s \cos\theta_j\right\} \\ &= Q\left[\sqrt{\frac{ST_s}{N_0}}\left(1 + \sqrt{\frac{2J_0}{S}}\,\cos\theta_j\right)\right]. \end{aligned} \tag{16}$$

Finally, the unconditional average probability of symbol error $\bar{P}_{E_J}$ for symbol intervals which are jammed is obtained by averaging $\bar{P}_E(\theta_j)$ of (15) over the uniform distribution of θ_j. Thus,

$$\bar{P}_{E_J} = \frac{1}{2\pi}\int_0^{2\pi} [P_s(\theta_j) + P_c(\theta_j) - P_s(\theta_j)P_c(\theta_j)]\,d\theta_j. \tag{17}$$

Recognizing that, for a QPSK signal, the symbol time T_s is twice the bit time T_b, letting $E_b = ST_b$ denote the bit energy, we then have

$$\frac{ST_s}{N_0} = \frac{2ST_b}{N_0} = \frac{2E_b}{N_0}. \tag{18}$$

Furthermore, from (4) and (5),

$$\frac{2J_0}{S} = \frac{2J}{\alpha NS}. \tag{19}$$

Now, if the hop frequency slots are $1/T_s$ wide, in terms of the total hop frequency band W and the number of hop slots N in that band, we then have

$$N = \frac{W}{1/T_s} = WT_s = 2WT_b. \tag{20}$$

Substituting (20) into (19) gives

$$\frac{2J_0}{S} = \frac{J/W}{\alpha ST_b} = \frac{J/W}{\alpha E_b} \triangleq \frac{N_J}{\alpha E_b}. \tag{21}$$

The quantity J/W represents the *effective jammer power spectral density* in the hop band; thus, we have introduced the notation N_J to represent this quantity.

Finally, rewriting (16) using (18) and (21) gives

$$\begin{aligned} P_s(\theta_j) &= Q\left[\sqrt{\frac{2E_b}{N_0}}\left(1 - \sqrt{\frac{N_J}{\alpha E_b}}\,\sin\theta_j\right)\right] \\ P_c(\theta_j) &= Q\left[\sqrt{\frac{2E_b}{N_0}}\left(1 + \sqrt{\frac{N_J}{\alpha E_b}}\,\cos\theta_j\right)\right] \end{aligned} \tag{22}$$

[4] The function $Q(x) = (1/\sqrt{2\pi})\int_x^\infty \exp(-y^2/2)dy$ is the Gaussian probability integral.

For the fraction $(1-\alpha)$ of symbol (hop) intervals where the jammer is absent, the average symbol error probability is given by the well-known result [1]

$$\bar{P}_{E_0} = 2Q\left(\sqrt{\frac{2E_b}{N_0}}\right) - Q^2\left(\sqrt{\frac{2E_b}{N_0}}\right) \tag{23}$$

Thus, the average error probability over all symbols (jammed and unjammed) is simply

$$\bar{P}_E = \alpha\bar{P}_{E_J} + (1-\alpha)\bar{P}_{E_0} \tag{24}$$

where $\bar{P}_{E_J}$ is given by (17), together with (22), and $\bar{P}_{E_0}$ is given in (23).

Before presenting numerical results illustrating the evaluation of (24), it is of interest to examine its limiting behavior as $N_0 \to 0$. Since

$$\lim_{\frac{E_b}{N_0}\to\infty} Q\left(\sqrt{\frac{2E_b}{N_0}}\,x\right) = \frac{1-\operatorname{sgn} x}{2} \tag{25}$$

where sgn x is the signum function defined by

$$\operatorname{sgn} x = \begin{cases} 1; & x>0 \\ -1; & x<0 \end{cases} \tag{26}$$

then clearly

$$\lim_{\frac{E_b}{N_0}\to\infty} \bar{P}_{E_0} = 0. \tag{27}$$

Also, from (22), for $N_J/\alpha E_b < 1$,

$$\left.\begin{aligned} &\lim_{\frac{E_b}{N_0}\to\infty} P_s(\theta_j) = 0 \\ &\lim_{\frac{E_b}{N_0}\to\infty} P_c(\theta_j) = 0 \end{aligned}\right\} \quad \text{for all } \theta_j \text{ in } (0, 2\pi). \tag{28}$$

For $1 < N_J/\alpha E_b < 2$

$$\lim_{\frac{E_b}{N_0}\to\infty} P_s(\theta_j) = \begin{cases} 1; & \sin^{-1}\sqrt{\dfrac{\alpha E_b}{N_j}} < \theta_j < \pi - \sin^{-1}\sqrt{\dfrac{\alpha E_b}{N_J}} \\ 0; & \text{elsewhere in } (0, 2\pi) \end{cases}$$

$$\lim_{\frac{E_b}{N_0}\to\infty} P_c(\theta_j) = \begin{cases} 1; & \pi - \cos^{-1}\sqrt{\dfrac{\alpha E_b}{N_J}} < \theta_j < \pi + \cos^{-1}\sqrt{\dfrac{\alpha E_b}{N_J}} \\ 0; & \text{elsewhere in } (0, 2\pi) \end{cases}$$

$$\lim_{\frac{E_b}{N_0}\to\infty} P_s(\theta_j)P_c(\theta_j) = 0 \qquad \text{for all } \theta_j \text{ in } (0, 2\pi). \tag{29}$$

For $N_J/\alpha E_b > 2$, the limiting forms of $P_s(\theta_j)$ and $P_c(\theta_j)$ are still given by (29), but

$$\lim_{\frac{E_b}{N_0}\to\infty} P_s(\theta_j)P_c(\theta_j) = \begin{cases} 1; & \pi - \cos^{-1}\sqrt{\dfrac{\alpha E_b}{N_J}} < \theta_j < \pi - \sin^{-1}\sqrt{\dfrac{\alpha E_b}{N_J}} \\ 0; & \text{elsewhere in } (0, 2\pi) \end{cases} \tag{30}$$

Thus, substituting (28)-(30) in (17) and carrying out the integration results in

$$\lim_{\frac{E_b}{N_0}\to\infty} \bar{P}_{E_J} = \begin{cases} 0; & \dfrac{\alpha E_b}{N_J} > 1 \\ \dfrac{2}{\pi}\cos^{-1}\sqrt{\dfrac{\alpha E_b}{N_J}}; & \frac{1}{2} < \dfrac{\alpha E_b}{N_J} < 1 \\ \dfrac{1}{\pi}\cos^{-1}\sqrt{\dfrac{\alpha E_b}{N_J}} + \dfrac{1}{4}; & 0 < \dfrac{\alpha E_b}{N_J} < \frac{1}{2}. \end{cases} \tag{31}$$

This result can also be obtained directly from the graphical interpretation given in Fig. 3. Finally, substituting (27) and (31) in (24) gives the desired limiting behavior for the average symbol error probability, namely

$$\lim_{\frac{E_b}{N_0}\to\infty} \bar{P}_E = \begin{cases} 0; & \dfrac{\alpha E_b}{N_J} > 1 \\ \dfrac{2\alpha}{\pi}\cos^{-1}\sqrt{\dfrac{\alpha E_b}{N_J}}; & \frac{1}{2} < \dfrac{\alpha E_b}{N_J} < 1 \\ \dfrac{\alpha}{\pi}\cos^{-1}\sqrt{\dfrac{\alpha E_b}{N_J}} + \dfrac{\alpha}{4}; & 0 < \dfrac{\alpha E_b}{N_J} < \frac{1}{2}. \end{cases} \tag{32}$$

The partial-band fraction α corresponding to the worst-

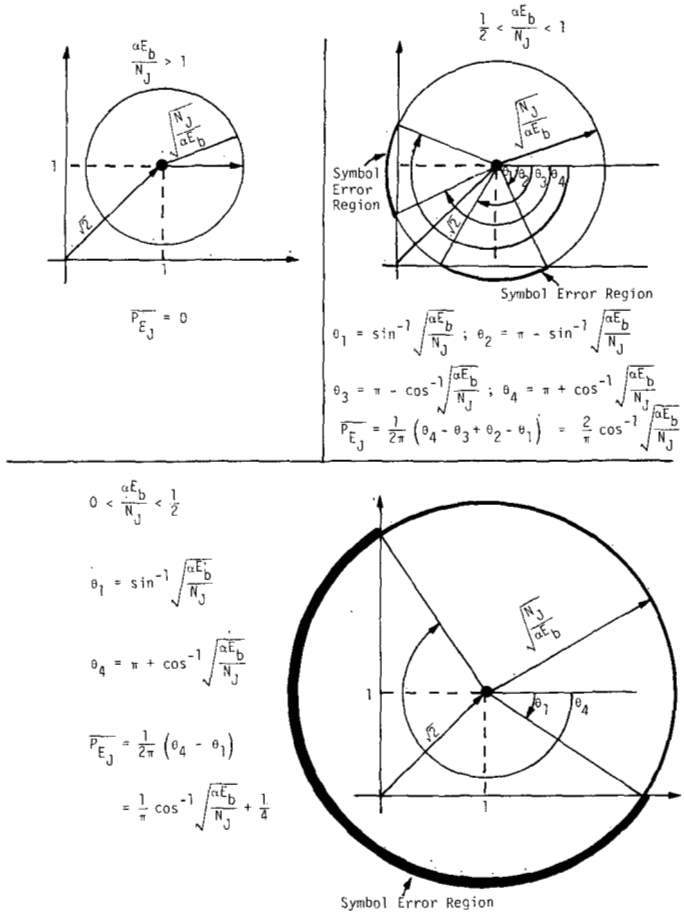

Fig. 3. Graphical interpretation of (31).

case jammer (maximum $\bar{P}_E$) can be obtained by differentiating (32) with respect to α and equating to zero. Assuming that, for a fixed E_b/N_J, this worst-case α occurs when $1/2 < \alpha E_b/N_J < 1$, then

$$\frac{d}{d\alpha}\left[\frac{2\alpha}{\pi}\cos^{-1}\sqrt{\frac{\alpha E_b}{N_J}}\right] = 0 \tag{33}$$

or

$$\cos^{-1}\sqrt{\frac{\alpha E_b}{N_J}} = \frac{1}{2}\sqrt{\frac{\frac{\alpha E_b}{N_J}}{1-\frac{\alpha E_b}{N_j}}}. \tag{34}$$

Alternately, since $\cos^{-1} x = \tan^{-1}(\sqrt{1-x^2}/x)$, we get the transcendental equation

$$\tan^{-1} Z = \frac{1}{2Z} \tag{35}$$

where

$$Z = \sqrt{\frac{1-\frac{\alpha E_b}{N_J}}{\frac{\alpha E_b}{N_J}}}. \tag{36}$$

The solution to (35) may be numerically found to be

$$Z = 0.7654 \tag{37}$$

or[5]

$$\alpha = \frac{0.6306}{E_b/N_J}. \tag{38}$$

Substituting (38) into (32) gives the limiting average symbol error probability performance corresponding to the worst-case jammer, namely

$$\lim_{\frac{E_b}{N_0}\to\infty} \bar{P}_{E\max} = \frac{0.2623}{E_b/N_J}. \tag{39}$$

The final step in the characterization of the performance of FH-QPSK in the presence of multitone jamming is the conversion of average symbol error probability to average bit error probability. If one encodes the information symbols using a Gray code, the average bit error probability $\bar{P}_b$ for a multiple phase shift keyed (MPSK) signal is then approximated for large E_b/N_0 by

$$\bar{P}_b \cong \frac{\bar{P}_E}{\log_2 M} \tag{40}$$

where $\log_2 M$ is the number of bits/symbol. The approximation in (40) refers to the fact that only errors in symbols whose corresponding signal phases are adjacent to that of the transmitted signal are accounted for. Since a Gray code has the property that adjacent symbols differ in only a single bit, then an error in an adjacent symbol is accompanied by one and only one bit error.

Since QPSK is the particular case of MPSK corresponding to $M = 4$, then from (40)

$$\bar{P}_b \cong \tfrac{1}{2}\bar{P}_E \tag{41}$$

where $\bar{P}_E$ is given by (24) or its limiting form in (32).

Fortunately, for the case of QPSK, it is straightforward to account for the diagonal symbol errors which result in two bit errors and, thus, arrive at an *exact* expression for $\bar{P}_b$. In fact, $\bar{P}_b$ for QPSK is identical to $\bar{P}_b$ for binary PSK (BPSK) and is given by

$$\bar{P}_b = \alpha\left[\frac{1}{2\pi}\int_0^{2\pi} P_s(\theta_j)\,d\theta_j\right] + (1-\alpha)Q\left(\sqrt{\frac{2E_b}{N_0}}\right)$$
$$= \alpha\left[\frac{1}{2\pi}\int_0^{2\pi} P_c(\theta_j)\,d\theta_j\right] + (1-\alpha)Q\left(\sqrt{\frac{2E_b}{N_0}}\right) \tag{42}$$

[5] Note that, since q and N are integers, then α as defined in (5) is not a continuous variable. Thus, for a given N, the true worst-case α would be the rational number nearest to (38) which yields an integer value of q. Also note that, for $E_b/N_J < 0.6306$, (38) would result in $\alpha > 1$, which has no physical meaning. Thus, for $E_b/N_J < 0.6306$, we take $\alpha = 1$ (full-band jamming) as the worst case.

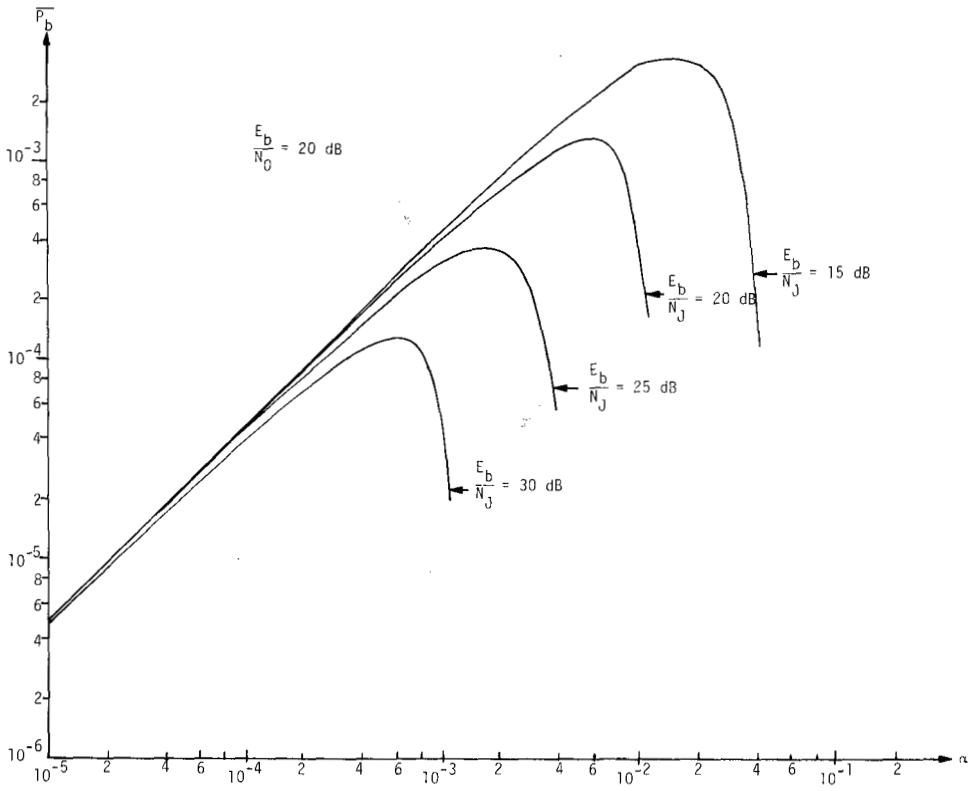

Fig. 4. $\bar{P}_b$ versus α—FH-QPSK (tone jamming).

where $P_s(\theta_j)$ and $P_c(\theta_j)$ are given in (22). Thus, comparing the approximate result of (41) [using (17), (22), and (24)] with the exact result of (42), we observe that the difference between the two resides in the terms resulting from the *product* of error probabilities, namely

$$\frac{1}{2\pi}\int_0^{2\pi} P_s(\theta_j)P_c(\theta_j)\,d\theta_j$$

and $Q^2(\sqrt{2E_b/N_0})$. Also, by analogy with (32), the exact limiting form of $\bar{P}_b$ becomes

$$\lim_{\frac{E_b}{N_0}\to\infty} \bar{P}_b = \begin{cases} 0; & \dfrac{\alpha E_b}{N_J} > 1 \\ \dfrac{\alpha}{\pi}\cos^{-1}\sqrt{\dfrac{\alpha E_b}{N_J}}; & 0 < \dfrac{\alpha E_b}{N_J} < 1 \end{cases} \tag{43}$$

with a worst-case α as in (38) and corresponding maximum error probability

$$\lim_{\frac{E_b}{N_0}\to\infty} \bar{P}_{b\max} = \frac{0.1311}{E_b/N_J}. \tag{44}$$

Fig. 4 is a typical plot of $\bar{P}_b$ versus α, with E_b/N_J as a parameter for the case $E_b/N_0 = 20$ dB. It is seen that, for fixed E_b/N_0 and E_b/N_J, there exists a value of α which maximizes $\bar{P}_b$ and thus represents the worst-case multitone jammer situation. In the limit, as E_b/N_0 approaches infinity, this value of α becomes equal to that given by (38). Fig. 5 is a plot of worst-case α versus E_b/N_J, with E_b/N_0 as a parameter. Fig. 6 illustrates the corresponding plot of $\bar{P}_{b\max}$ versus E_b/N_J, with E_b/N_0 fixed.

III. PERFORMANCE OF FH-QASK IN THE PRESENCE OF PARTIAL-BAND MULTITONE JAMMING

An FH-QASK-M signal is characterized by transmitting

$$s^{(i)}(t) = \sqrt{2}\delta[b_n \cos \omega_H{}^{(i)}t + a_m \sin \omega_H{}^{(i)}t] \tag{45}$$

in the ith signaling interval. The total number of signals possible M is typically the square of an even number K, and the quadrature amplitudes a_m and b_n take on equally likely values m and n, respectively, with $m, n = \pm 1, \pm 3, \cdots, \pm(K-1)$. Also, δ is a parameter which is related to the average power S of the signal set by

$$S = \tfrac{2}{3}(K^2 - 1)\delta^2. \tag{46}$$

Analogous to the step leading to (11), we can arrive at expressions for the in-phase and quadrature decision variables, namely

$$z_I = a_i\delta T_s - \sqrt{J_0}T_s \sin\theta_j + N_I$$

$$z_Q = b_i\delta T_s + \sqrt{J_0}T_s \cos\theta_j + N_Q. \tag{47}$$

The QASK receiver estimates of a_i and b_i are obtained by passing z_I and z_Q through K-level quantizers

$$\hat{a}_i = Q_K(z_I); \quad \hat{b}_i = Q_K(Z_Q) \tag{48}$$

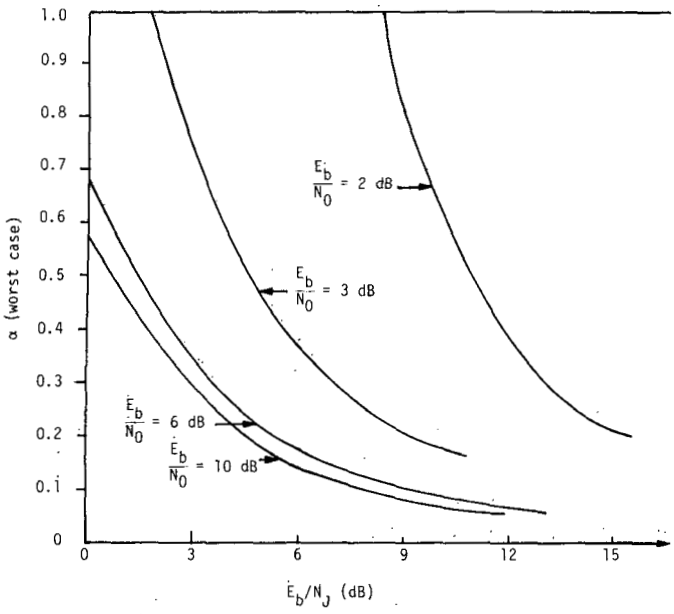

Fig. 5. Worst-case α versus E_b/N_J–FH-QPSK (tone jamming).

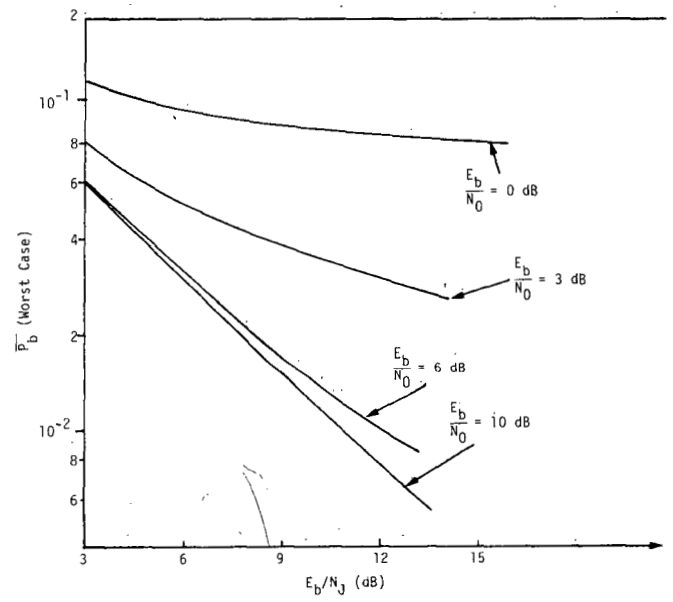

Fig. 6. Worst-case $\bar{P}_b$ versus E_b/N_J–FH-QPSK (tone jamming).

where

$$Q_K(x) = \begin{cases} 1; & 0 \leq x \leq 2\delta T_s \\ 3; & 2\delta T_s \leq x \leq 4\delta T_s \\ \vdots & \\ (K-3); & (K-4)\delta T_s \leq x \leq (K-2)\delta T_s \\ (K-1); & (K-2)\delta T_s \leq x \leq \infty \end{cases} \tag{49}$$

and $Q_K(x) = -Q_K(-x)$. Hence, given a_i, b_i, and θ_j, the probability that the ith symbol is in error is the probability that $\hat{a}_i$ or $\hat{b}_i$ is in error. Thus, once again, (14) is valid. Here, however, we must compute (14) for the $K^2/4$ points in any quadrant in order to obtain the average probability of symbol error conditioned on the jammer phase. Thus, using QASK-16 ($K = 4$) as an example, we have

$$\begin{aligned} \text{Prob}\{\hat{a}_i \neq a_i\} &\triangleq P_s(\theta_j) \\ &= \tfrac{1}{2}\,\text{Prob}\{0 > z_I > 2\delta T_s \mid a_i = 1\} \\ &\quad + \tfrac{1}{2}\,\text{Prob}\{z_I < 2\delta T_s \mid a_i = 3\} \\ \text{Prob}\{\hat{b}_i \neq b_i\} &\triangleq P_c(\theta_j) \\ &= \tfrac{1}{2}\,\text{Prob}\{0 > z_Q > 2\delta T_s \mid b_i = 1\} \\ &\quad + \tfrac{1}{2}\,\text{Prob}\{z_Q < 2\delta T_s \mid b_i = 3\} \end{aligned} \tag{50}$$

or

$$\begin{aligned} P_s(\theta_j) &= \tfrac{1}{2}\,\text{Prob}\{\delta T_s + \sqrt{J_0}\,T_s \sin\theta_j \\ &\quad < N_I < -\delta T_s + \sqrt{J_0}\,T_s \sin\theta_j\} \\ &\quad + \tfrac{1}{2}\,\text{Prob}\{N_I < -\delta T_s + \sqrt{J_0}\,T_s \sin\theta_j\} \\ &= Q\left[\sqrt{\frac{2\delta^2 T_s}{N_0}}\left(1 - \sqrt{\frac{J_0}{\delta^2}}\sin\theta_j\right)\right] \\ &\quad + \tfrac{1}{2}Q\left[\sqrt{\frac{2\delta^2 T_s}{N_0}}\left(1 + \sqrt{\frac{J_0}{\delta^2}}\sin\theta_j\right)\right] \end{aligned} \tag{51}$$

and

$$\begin{aligned} P_c(\theta_j) &= \tfrac{1}{2}\text{Prob}\{\delta T_s - \sqrt{J_0}\,T_s \cos\theta_j \\ &\quad < N_Q < -\delta T_s - \sqrt{J_0}\,T_s \cos\theta_j\} \\ &\quad + \tfrac{1}{2}\,\text{Prob}\{N_Q < -\delta T_s - \sqrt{J_0}\,T_s \cos\theta_j\} \\ &= Q\left[\sqrt{\frac{2\delta^2 T_s}{N_0}}\left(1 + \sqrt{\frac{J_0}{\delta^2}}\cos\theta_j\right)\right] \\ &\quad + \tfrac{1}{2}Q\left[\sqrt{\frac{2\delta^2 T_s}{N_0}}\left(1 - \sqrt{\frac{J_0}{\delta^2}}\cos\theta_j\right)\right]. \end{aligned} \tag{52}$$

Letting $K = 4$ in (46) and recognizing that $T_s = 4T_b$, we now have

$$\frac{2\delta^2 T_s}{N_0} = \frac{ST_s}{5N_0} = 2\left(\frac{2}{5}\frac{ST_b}{N_0}\right) \triangleq \frac{2E_b'}{N_0} \tag{53}$$

where

$$E_b' \triangleq \tfrac{2}{5}E_b. \tag{54}$$

Also,

$$\frac{J_0}{\delta^2} = \frac{10J}{\alpha NS} = \frac{10J}{\alpha(4WT_b)S} = \frac{J/W}{\alpha E_b'} = \frac{N_J}{\alpha E_b'}. \tag{55}$$

Finally, then, the unconditional average probability of symbol error $\bar{P}_{E_J}$ for symbol intervals which are jammed is given by

(17) with (for QASK-16)

$$P_s(\theta_j) = Q\left[\sqrt{\frac{2E_b'}{N_0}}\left(1 - \sqrt{\frac{N_J}{\alpha E_b'}}\sin\theta_j\right)\right] + \tfrac{1}{2}Q\left[\sqrt{\frac{2E_b'}{N_0}}\left(1 + \sqrt{\frac{N_J}{\alpha E_b'}}\sin\theta_j\right)\right]$$

$$P_c(\theta_j) = Q\left[\sqrt{\frac{2E_b'}{N_0}}\left(1 + \sqrt{\frac{N_J}{\alpha E_b'}}\cos\theta_j\right)\right] + \tfrac{1}{2}Q\left[\sqrt{\frac{2E_b'}{N_0}}\left(1 - \sqrt{\frac{N_J}{\alpha E_b'}}\cos\theta_j\right)\right]. \quad (56)$$

For symbol intervals which are not jammed, the average symbol error probability is given by the well-known result [2]

$$\bar{P}_{E_0} = 3Q\left(\sqrt{\frac{2E_b'}{N_0}}\right) - \tfrac{9}{4}Q^2\left(\sqrt{\frac{2E_b'}{N_0}}\right). \quad (57)$$

Thus, the average error probability over all symbols is once again given by (24) with, however, $\bar{P}_{E_J}$ of (17) together with (56) and $\bar{P}_{E_0}$ of (57).

As was done for FH-QPSK, one can compute the limiting performance of FH-QASK as E_b/N_0 approaches infinity. In particular, using (25) in (56), we obtain the following result.

For $N_J/\alpha E_b' < 1$

$$\left.\begin{aligned}&\lim_{\frac{E_b}{N_0}\to\infty} P_s(\theta_j) = 0\\ &\lim_{\frac{E_b}{N_0}\to\infty} P_c(\theta_j) = 0\end{aligned}\right\} \text{ for all } \theta_j \text{ in } (0, 2\pi) \quad (58)$$

which is identical to the result obtained for FH-QPSK in (28).

For $1 < N_J/\alpha E_b' < 2$

$$\lim_{\frac{E_b}{N_0}\to\infty} P_s(\theta_j) = \begin{cases} 1; & \sin^{-1}\sqrt{\frac{\alpha E_b'}{N_J}} < \theta_j < \pi - \sin^{-1}\sqrt{\frac{\alpha E_b'}{N_J}} \\ \frac{1}{2}; & \pi + \sin^{-1}\sqrt{\frac{\alpha E_b'}{N_J}} < \theta_j < 2\pi - \sin^{-1}\sqrt{\frac{\alpha E_b'}{N_J}} \\ 0; & \text{elsewhere in } (0, 2\pi) \end{cases}$$

$$\lim_{\frac{E_b}{N_0}\to\infty} P_c(\theta_j) = \begin{cases} 1; & \pi - \cos^{-1}\sqrt{\frac{\alpha E_b'}{N_J}} < \theta_j < \pi + \cos^{-1}\sqrt{\frac{\alpha E_b'}{N_J}} \\ \frac{1}{2}; & 0 < \theta_j < \cos^{-1}\sqrt{\frac{\alpha E_b'}{N_J}} \\ \frac{1}{2}; & 2\pi - \cos^{-1}\sqrt{\frac{\alpha E_b'}{N_J}} < \theta_j < 2\pi \\ 0; & \text{elsewhere in } (0, 2\pi) \end{cases}$$

$$\lim_{\frac{E_b}{N_0}\to\infty} P_s(\theta_j)P_c(\theta_j) = 0 \quad \text{for all } \theta_j \text{ in } (0, 2\pi). \quad (59)$$

For $N_J/\alpha E_b' > 2$, the limiting forms of $P_s(\theta_j)$ and $P_c(\theta_j)$ are still given by (56) but

$$\lim_{\frac{E_b}{N_0}\to\infty} P_s(\theta_j)P_c(\theta_j) = \begin{cases} \frac{1}{2}; & \sin^{-1}\sqrt{\frac{\alpha E_b'}{N_J}} < \theta_j < \cos^{-1}\sqrt{\frac{\alpha E_b'}{N_J}} \\ 1; & \pi - \cos^{-1}\sqrt{\frac{\alpha E_b'}{N_J}} < \theta_j < \pi - \sin^{-1}\sqrt{\frac{\alpha E_b'}{N_J}} \\ \frac{1}{2}; & \pi + \sin^{-1}\sqrt{\frac{\alpha E_b'}{N_J}} < \theta_j < \pi + \cos^{-1}\sqrt{\frac{\alpha E_b'}{N_J}} \\ \frac{1}{4}; & 2\pi - \cos^{-1}\sqrt{\frac{\alpha E_b'}{N_J}} < \theta_j < 2\pi - \sin^{-1}\sqrt{\frac{\alpha E_b'}{N_J}} \\ 0; & \text{elsewhere in } (0, 2\pi). \end{cases} \quad (60)$$

Thus, substituting (58)-(60) in (17) and carrying out the

integration results in

$$\lim_{\frac{E_b}{N_0}\to\infty} \bar{P}_{E_J} = \begin{cases} 0; & \frac{\alpha E_b'}{N_J} > 1 \\ \frac{3}{\pi}\cos^{-1}\sqrt{\frac{\alpha E_b'}{N_J}}; & \frac{1}{2} < \frac{\alpha E_b'}{N_J} < 1 \\ \frac{3}{4\pi}\cos^{-1}\sqrt{\frac{\alpha E_b'}{N_J}} + \frac{9}{16}; & 0 < \frac{\alpha E_b'}{N_J} < \frac{1}{2}. \end{cases} \quad (61)$$

This result could also be obtained directly using a graphical interpretation analogous to Fig. 3. Finally, realizing that (27) also applies to $\bar{P}_{E_0}$ of (57), substituting (27) and (61) into (24) then gives the desired limiting behavior of the average symbol error probability of QASK-16, namely

$$\lim_{\frac{E_b}{N_0}\to\infty} \bar{P}_E = \begin{cases} 0; & \frac{\alpha E_b'}{N_J} > 1 \\ \frac{3\alpha}{\pi}\cos^{-1}\sqrt{\frac{\alpha E_b'}{N_J}}; & \frac{1}{2} < \frac{\alpha E_b'}{N_J} < 1 \\ \frac{3\alpha}{4\pi}\cos^{-1}\sqrt{\frac{\alpha E_b'}{N_J}} + \frac{9\alpha}{16}; & 0 < \frac{\alpha E_b'}{N_J} < \frac{1}{2}. \end{cases} \quad (62)$$

To determine the worst-case jamming situation, we again differentiate $\bar{P}_E$, now given by (62), with respect to α and equate to zero. Recognizing that the expression for $\bar{P}_E$ of QASK-16 in the interval $1/2 < \alpha E_b'/N_J < 1$ is 3/2 times that for $\bar{P}_E$ of QPSK in the interval $1/2 < \alpha E_b/N_J < 1$, we can immediately observe that the worst-case α is now

$$\alpha = \frac{0.6306}{E_b'/N_J} \quad (63)$$

and the corresponding worst-case average symbol error probability performance is

$$\lim_{\frac{E_b}{N_0}\to\infty} \bar{P}_{E_{\max}} = \frac{3}{2}\left(\frac{0.2623}{E_b'/N_J}\right) = \frac{0.9835}{E_b/N_J} \quad (64)$$

where we have also made use of (54).

If one encodes the QASK symbols with a perfect Gray code, then accounting only for adjacent symbol errors (which is equivalent to one bit error per symbol error), the average bit error probability for large E_b/N_0 and $\alpha E_b/N_J$ is related to the average symbol error probability by (40), where now $M = K^2$ is the total number of symbols or $\log_2 M = \log_2 K^2$ is the number of bits/symbol. Clearly, for QASK-16

$$\bar{P}_b \cong \tfrac{1}{4}\bar{P}_E \qquad (\text{for } E_b/N_0 \gg 1, \alpha E_b/N_J \gg 1). \quad (65)$$

Equation (65) provides an optimistic estimate of $\bar{P}_b$. The exact expression can be calculated via the fact that QASK-16 is obtained from independent amplitude shift keying on two quadrature components of a carrier. Assuming a perfectly coherent receiver, no interchannel effects exist in the demodulation process. Hence, the bit error probability $\bar{P}_b$ for QASK-16 is identical to $\bar{P}_b$ for each individual channel and is given by (Appendix)

$$\bar{P}_b = \alpha\bar{P}_{b_J} + (1-\alpha)\bar{P}_{b_0} \quad (66)$$

where

$$\bar{P}_{b_J} = \frac{1}{4\pi}\int_0^{2\pi} [P_c(\theta_j) + P_c^*(\theta_j)]\, d\theta_j \quad (67)$$

with $P_c(\theta_j)$ as in (56) and $P_c^*(\theta_j)$ equal to

$$P_c^*(\theta_j) = Q\left[\sqrt{\frac{2E_b'}{N_0}}\left(3 + \sqrt{\frac{N_J}{\alpha E_b'}}\cos\theta_j\right)\right] - \tfrac{1}{2}Q\left[\sqrt{\frac{2E_b'}{N_0}}\left(5 + \sqrt{\frac{N_J}{\alpha E_b'}}\cos\theta_j\right)\right]. \quad (68)$$

Furthermore, $\bar{P}_{b_0}$ of (66) represents the average bit error probability in the presence of noise only and is given by

$$\bar{P}_{b_0} = \tfrac{3}{4}Q\left[\sqrt{\frac{2E_b'}{N_0}}\right] + \tfrac{1}{2}Q\left[3\sqrt{\frac{2E_b'}{N_0}}\right] - \tfrac{1}{4}Q\left[5\sqrt{\frac{2E_b'}{N_0}}\right]. \quad (69)$$

Once again before presenting numerical results illustrating the evaluation of (66), it is of interest to examine its limiting behavior as $N_0 \to 0$. Following the approach taken for FH-QPSK, we can arrive at the following result.

$$\lim_{\frac{E_b}{N_0}\to\infty} \bar{P}_b = \begin{cases} 0; & \frac{\alpha E_b'}{N_J} > 1 \\ \frac{3\alpha}{4\pi}\cos^{-1}\sqrt{\frac{\alpha E_b'}{N_J}}; & \frac{1}{9} < \frac{\alpha E_b'}{N_J} < 1 \\ \frac{3\alpha}{4\pi}\cos^{-1}\sqrt{\frac{\alpha E_b'}{N_J}} + \frac{2\alpha}{4\pi}\cos^{-1}\sqrt{\frac{9\alpha E_b'}{N_J}}; & \frac{1}{25} < \frac{\alpha E_b'}{N_J} < \frac{1}{9} \\ \frac{3\alpha}{4\pi}\cos^{-1}\sqrt{\frac{\alpha E_b'}{N_J}} + \frac{2\alpha}{4\pi}\cos^{-1}\sqrt{\frac{9\alpha E_b'}{N_J}} - \frac{\alpha}{\pi}\cos^{-1}\sqrt{\frac{25\alpha E_b'}{N_J}}; & 0 < \frac{\alpha E_b'}{N_J} < \frac{1}{25}. \end{cases} \quad (70)$$

The partial band fraction α corresponding to the worst case jammer (maximum $\bar{P}_b$) is obtained by differentiating (70) with respect to α and equating to zero. Assuming that for a fixed E_b'/N_J, this worst case α occurs when $1/9 < \alpha E_b'/N_J < 1$, then the solution to the transcendental equation which results from the differentiation is identical to (38) with E_b replaced by E_b', namely

$$\alpha = \frac{0.6306}{E_b'/N_J} = \frac{1.5765}{E_b/N_J}. \tag{71}$$

Substituting (71) into (70) gives the limiting average bit error probability performance corresponding to the worst-case jammer, namely

$$\lim_{\frac{E_b}{N_0}\to\infty} \bar{P}_{b_{\max}} = \frac{0.0984}{E_b'/N_J} = \frac{0.2459}{E_b/N_J}. \tag{72}$$

Figs. 7-9 are the numerical evaluations of FH-QASK-16 performance which are analogous to those in Figs. 4-6 characterizing FH-QPSK.

IV. PERFORMANCE OF FH-QPSK IN THE PRESENCE OF PARTIAL-BAND NOISE JAMMING

Now assume that the jammer $j(t)$ spreads his total power J uniformly across a fraction α of the total hop frequency band W. Then, insofar as the data demodulation process is concerned, the jammer appears as an additional additive noise source of power spectral density

$$N_J' = \frac{J}{\alpha W} = \frac{N_J}{\alpha}. \tag{73}$$

Note that the power spectral density of the noise jammer defined in (73) is identical to the effective power spectral density defined for the multitone jammer in (21).

Since the jammer noise can be assumed to be independent of the background additive Gaussian noise, one can add their power spectral densities and use this sum to represent the total noise perturbing the receiver. Thus, the error probability performance of FH-QPSK in the presence of partial-band noise jamming is characterized by taking the well-known results for just an additive white Gaussian noise background and replacing N_0 by $N_0 + N_J'$.

Without going into great detail, we then see that the average symbol error probability is once again given by (24), with $\bar{P}_{E_0}$ as in (23) but, however,

$$\bar{P}_{E_J} = 2Q\left(\sqrt{\frac{2E_b}{N_0 + N_J'}}\right) - Q^2\left(\sqrt{\frac{2E_b}{N_0 + N_J'}}\right). \tag{74}$$

Substituting (73) into (74), we can rewrite $\bar{P}_{E_J}$ in the alternate form:

$$\bar{P}_{E_J} = 2Q\left(\left[\left(\frac{2E_b}{N_0}\right)^{-1} + \left(\frac{2\alpha E_b}{N_J}\right)^{-1}\right]^{-1/2}\right) - Q^2\left(\left[\left(\frac{2E_b}{N_0}\right)^{-1} + \left(\frac{2\alpha E_b}{N_J}\right)^{-1}\right]^{-1/2}\right). \tag{75}$$

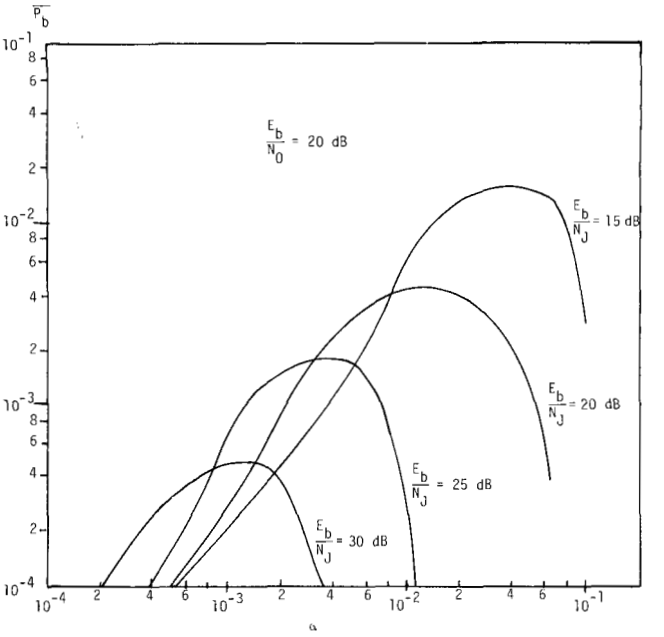

Fig. 7. $\bar{P}_b$ versus α for FH-QASK-16 in tone jamming with E_b/N_0 = 20 dB.

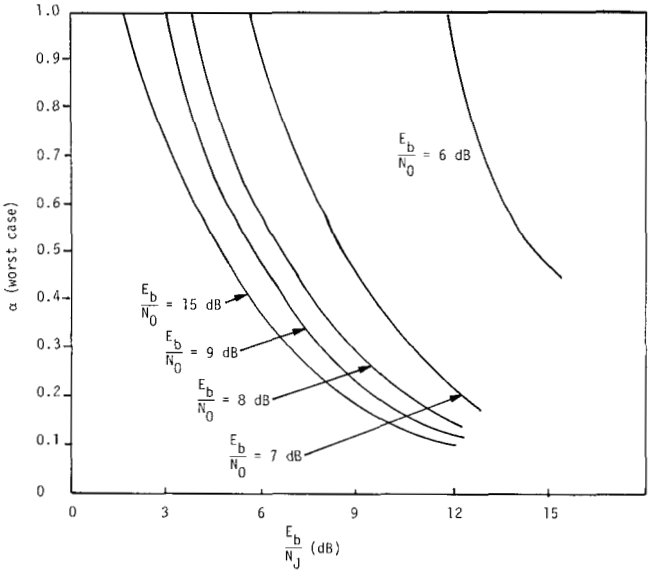

Fig. 8. Worst-case α versus E_b/N_J for FH-QASK-16 in tone jamming.

Also, the average bit error probability is now

$$\bar{P}_b = \alpha Q\left(\left[\left(\frac{2E_b}{N_0}\right)^{-1} + \left(\frac{2\alpha E_b}{N_J}\right)^{-1}\right]^{-1/2}\right) + (1-\alpha)Q\left(\sqrt{\frac{2E_b}{N_0}}\right) \tag{76}$$

which is identical to the result for noise jamming of FH-BPSK.

The limiting behavior of (76) as E_b/N_0 approaches infinity is easily seen to be

$$\lim_{\frac{E_b}{N_0}\to\infty} \bar{P}_b = \alpha Q\left(\sqrt{\frac{2\alpha E_b}{N_J}}\right). \tag{77}$$

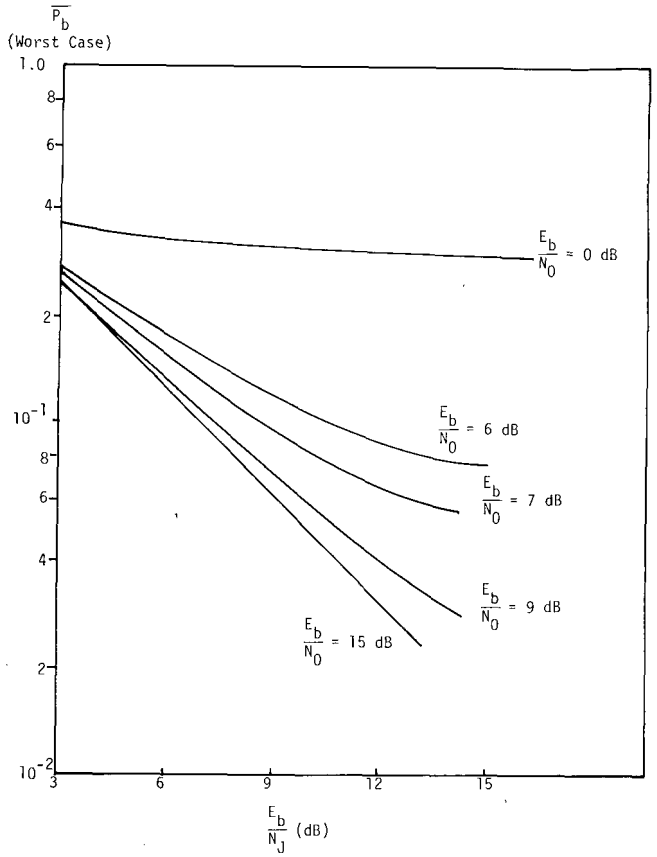

Fig. 9. Worst-case $\bar{P}_b$ versus E_b/N_J for FH-QASK-16 in tone jamming.

Differentiating (77) with respect to α and equating the result to zero gives the transcendental equation

$$Q\left(\sqrt{\frac{2\alpha E_b}{N_J}}\right)=\sqrt{\frac{\alpha E_b}{N_J}}\left(\frac{e^{-\alpha E_b/N_J}}{2\sqrt{\pi}}\right) \tag{78}$$

whose solution for α corresponds to the worst-case jammer situation. In particular, letting

$$x=\sqrt{\frac{\alpha E_b}{N_J}} \tag{79}$$

(78) then becomes

$$Q(\sqrt{2}x)=\frac{xe^{-x^2}}{2\sqrt{\pi}} \tag{80}$$

which, when solved numerically, yields

$$x=0.842. \tag{81}$$

Equating (79) and (81) gives the partial-band fraction for the worst-case jammer, namely[6]

$$\alpha=\frac{0.7090}{E_b/N_J} \tag{82}$$

[6] Comments similar to those in footnote 5 associated with (38) apply to this result.

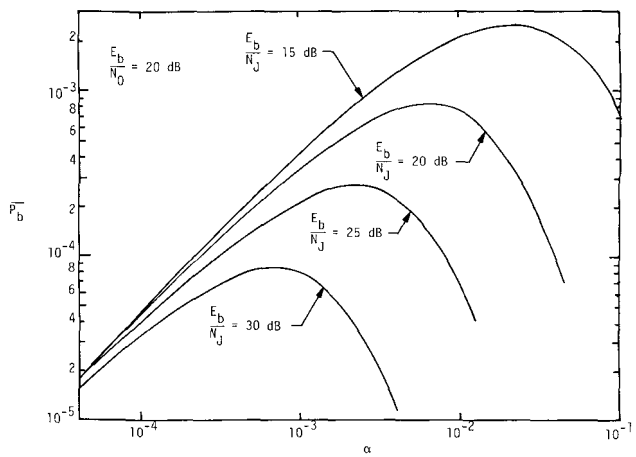

Fig. 10. $\bar{P}_b$ versus α for FH-QPSK (noise jamming) with E_b/N_0 = 20 dB.

and a corresponding maximum average bit error probability

$$\lim_{\frac{E_b}{N_0}\to\infty}\bar{P}_{b_{max}}=\frac{0.0829}{E_b/N_J}. \tag{83}$$

Figs. 10-12 characterize the performance of FH-QPSK in the presence of noise jamming, as computed from (76).

V. PERFORMANCE OF FH-QASK IN THE PRESENCE OF NOISE JAMMING

Assuming the same noise jammer model as that discussed in the previous section for FH-QPSK, the average symbol error probability of FH-QASK-16 is then given by (24), with $\bar{P}_{E_0}$ as in (57), but now

$$\bar{P}_{E_J}=3Q\left(\left[\left(\frac{2E_b'}{N_0}\right)^{-1}+\left(\frac{2\alpha E_b}{N_J}\right)^{-1}\right]^{-1/2}\right)-\tfrac{9}{4}Q^2\left(\left[\left(\frac{2E_b'}{N_0}\right)^{-1}+\left(\frac{2\alpha E_b'}{N_J}\right)^{-1}\right]^{-1/2}\right). \tag{84}$$

The limiting behavior of (24), together with (57) and (84) as E_b/N_0 approaches infinity, is simply

$$\lim_{\frac{E_b}{N_0}\to\infty}\bar{P}_E=3\alpha Q\left(\sqrt{\frac{2\alpha E_b'}{N_J}}\right)-\frac{9\alpha}{4}Q^2\left(\sqrt{\frac{2\alpha E_b'}{N_J}}\right) \tag{85}$$

which yields a partial-band fraction for the worst-case jammer given by the solution to

$$3Q(\sqrt{2}x)-3x\frac{e^{-x^2}}{2\sqrt{\pi}}-\tfrac{9}{4}Q^2(\sqrt{2}x)+\tfrac{9}{2}Q(\sqrt{2}x)\left[\frac{xe^{-x^2}}{2\sqrt{\pi}}\right]=0 \tag{86}$$

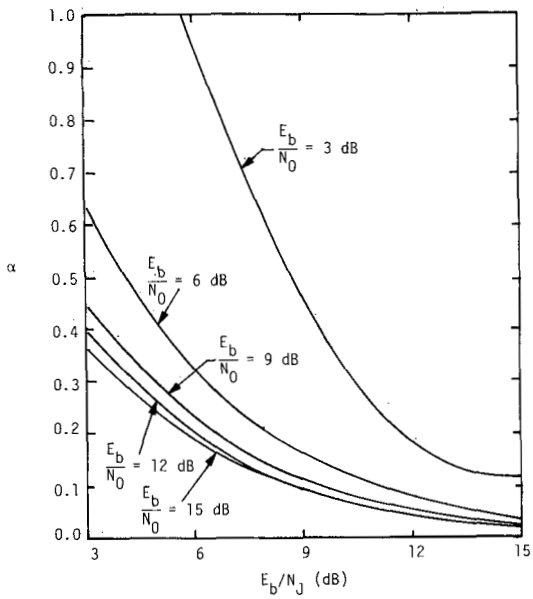

Fig. 11. Worst-case α versus E_b/N_J for FH-QPSK (noise jamming).

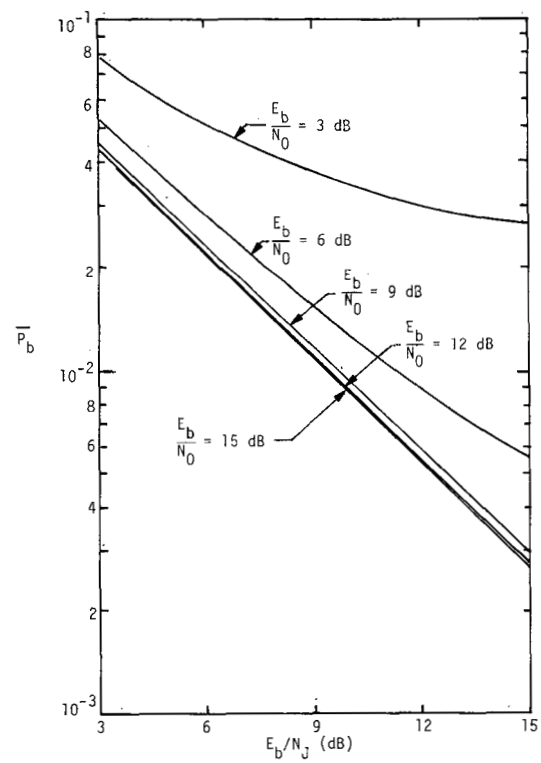

Fig. 12. Worst-case $\overline{P}_b$ versus E_b/N_J for FH-QPSK (noise jamming).

with

$$x = \sqrt{\frac{\alpha E_b'}{N_J}}. \tag{87}$$

Numerical solution of (86) yields[7]

$$\alpha = \frac{0.7921}{(\frac{2}{5})E_b/N_J} = \frac{1.9802}{E_b/N_J} \tag{88}$$

[7] Comments similar to those in footnote 5 associated with (38) apply to this result.

and a corresponding worst-case average symbol error probability

$$\lim_{\frac{E_b}{N_0}\to\infty} \overline{P}_{E_{\max}} = \frac{0.5700}{E_b/N_J}. \tag{89}$$

The average bit error probability $\overline{P}_b$ is obtained from (66), where $\overline{P}_{b_0}$ is given by (69) and $\overline{P}_{b_J}$ is given by

$$\overline{P}_{b_J} = \tfrac{3}{4}Q(x) + \tfrac{1}{2}Q(3x) - \tfrac{1}{4}Q(5x) \tag{90a}$$

with

$$x = \left[\left(\frac{2E_b'}{N_0}\right)^{-1} + \left(\frac{2\alpha E_b'}{N_J}\right)^{-1}\right]^{-1/2}. \tag{90b}$$

The limiting behavior of $\overline{P}_b$ as E_b/N_0 approaches infinity is then

$$\lim_{\frac{E_b}{N_0}\to\infty} \overline{P}_b = \alpha[\tfrac{3}{4}Q(x_\infty) + \tfrac{1}{2}Q(3x_\infty) - \tfrac{1}{4}Q(5x_\infty)] \tag{91a}$$

where x_∞ is the corresponding limit of x in (90b), namely

$$x_\infty = \sqrt{\frac{2\alpha E_b'}{N_J}}. \tag{91b}$$

The worst-case jammer is found through a procedure analogous to the one in Section IV. Under the aforementioned constraint $\alpha \leqslant 1$, the results are

$$\alpha = \frac{1.758}{E_b/N_J} \tag{92}$$

and a corresponding maximum average bit error probability of

$$\lim_{\frac{E_b}{N_0}\to\infty} \overline{P}_{b_{\max}} = \frac{0.1555}{E_b/N_J}. \tag{93}$$

It is interesting to note that the ratio $(\lim \overline{P}_{b_{\max}}/\lim \overline{P}_{E_{\max}})$ as computed from (89) and (93) is 0.2728, which is slightly higher than the approximate value of 1/4 as in (65). Furthermore, those limits are achieved for values of α [see (88) and (92)] which are different but relatively close.

Figs. 13-15 characterized the performance of FH-QASK-16 in the presence of noise jamming, as computed from the results given in this section.

In Fig. 13, the dotted line represents the locus of the maxima of $\overline{P}_b$ versus α, with E_b/N_J as a parameter. It can be seen that the value of 20 dB for E_b/N_0 is sufficiently high to warrant an almost linear relationship between $\overline{P}_{b_{\max}}$ and α, which closely conforms with the theoretically predicted

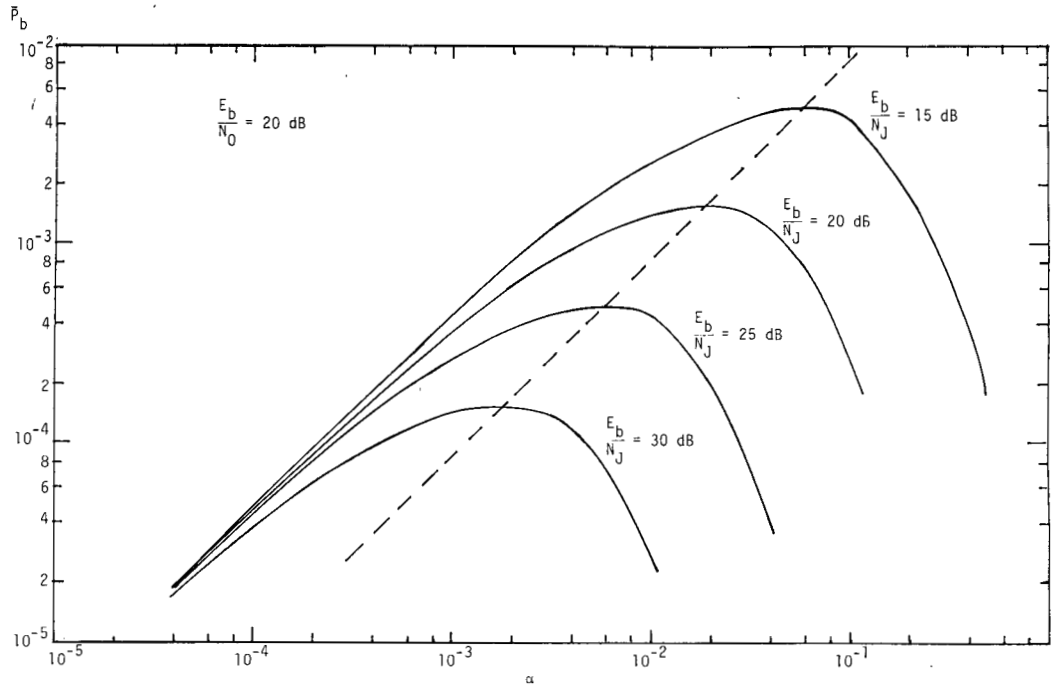

Fig. 13. $\bar{P}_b$ versus α for FH-QASK-16 in noise jamming with $E_b/N_0 = 20$ dB.

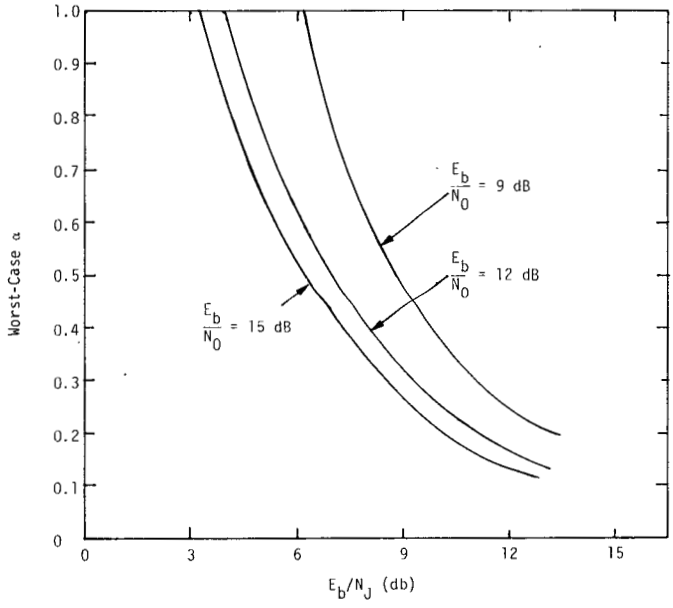

Fig. 14. Worst-case α versus E_b/N_J for FH-QASK-16 in noise jamming.

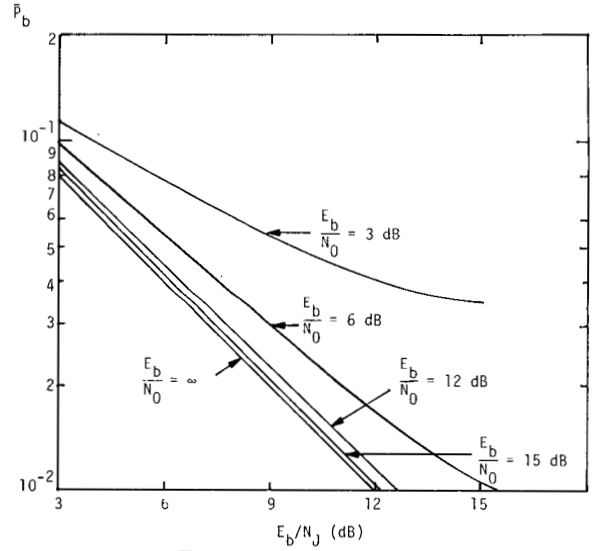

Fig. 15. Worst-case $\bar{P}_b$ versus E_b/N_J–FH-QASK-16 (noise jamming).

line [see (92) and (93)]

$$\lim_{\frac{E_b}{N_0}\to\infty} \bar{P}_{b_{\max}} = 0.0878\alpha.$$

VI. PERFORMANCE OF FH/PN-QPSK IN THE PRESENCE OF PARTIAL-BAND MULTITONE JAMMING

When a direct-sequence pseudonoise (PN) balanced modulation is superimposed on an FH-QPSK signal, each jammer tone of power J_0 is then spread over a bandwidth equal to the PN chip rate R_c. Let $R_s = 1/T_s$ be the information symbol rate and R_c/R_s represent the processing gain associated with the PN spreading, herein taken to be a large integer M. It follows from the assumption of a large processing gain that the spread tone jammer possesses a fairly flat[8] power spectral density within the data modulation bandwidth and is now caused to behave like a white noise jammer of spectral density

$$N_J' = J_0/R_c = J_0 T_c. \tag{94}$$

[8] The actual power spectral density of the despread tone is approximately of the form $(\sin x/x)^2$ where the main lobe has an RF bandwidth equal to twice the chip rate. Since the detection filter bandwidth is on the order of the data rate, which is much less than the chip rate, then the power spectral density can be assumed flat over this bandwidth.

Using (4) and (5), we can rewrite (94) as

$$N_J' = J/\alpha N R_c. \tag{95}$$

Since the hop frequency slots must now be R_c wide to accommodate the PN modulation,[9] in terms of the total hop frequency band W and the number of hop slots N in that band, we then have

$$N = W/R_c. \tag{96}$$

Combining (95) and (96) gives

$$N_J' = \frac{J/W}{\alpha} = \frac{N_J}{\alpha} \tag{97}$$

which is identical to (73) (the case of FH-QPSK in the presence of PB noise jamming) *independent of the chip rate* R_c.

The above discussion concerns the spectral characteristics of the spread tone jammer which, as concluded, resembles a white noise jammer with identical spectral density. We shall now discuss the assumptions and theoretical adjustments under which the spread tone jammer can also be treated as a *Gaussian* noise interference. Consider an FH/PN-QPSK demodulator, similar to the one in Fig. 2, where the despreading process now also includes a PN code correlator following the frequency dehopper. Let L represent the PN code length (in number of chips). Accounting for the effects of the spread jammer only (i.e., neglecting thermal noise), it follows that the decision variable z_I for the in-phase channel [see (11)] becomes

$$z_I = a_i\sqrt{\frac{S}{2}}\,T_s - \sqrt{J_0}\,\sin\theta_j C_{\mathrm{PN}} \tag{98}$$

where

$$C_{\mathrm{PN}} = \int_{(i-1)T_s}^{iT_s} \mathrm{PN}(t)\,dt \tag{99}$$

and PN(t) is the ±1 valued PN waveform. In deriving (98), ideal PN code synchronization at the receiver has been assumed. Recalling that the processing gain

$$\frac{R_c}{R_s} = \frac{T_s}{T_c} = (\text{integer})\,M \gg 1$$

it follows that the integral in (99) amounts to a partial correlation of the PN code [4], starting from some random phase, provided that the number M of integrated chips does not equal the code length L. Phrased differently, the conclusions to follow hold when $1 \ll M \ll L$ (or in a weaker sense when $1 \ll M$ modulo $L \ll L$). This is because, as is well known, the full-period integration of a PN code equals the constant $1/L$, in which case no randomness about C_{PN} exists. On the other hand, when L is very large, successive code chips can be considered almost independent, identically distributed ±1 valued random variables, in which case the condition $M \ll L$ would provide an approximate binomial distribution for the random variable C_{PN}. The additional constraint $M \gg 1$ then causes this binomial distribution to behave like a Gaussian distribution. The validity of the aforementioned Gaussian assumption for C_{PN} has been rigorously examined in [5] for a variety of PN and Gold codes, with sufficient evidence that it holds, at least approximately and for a wide class of such codes. Second-order statistics of C_{PN} under the long code assumption appear in [6].[10]

Let us now return to (98). Conditioned on the $(0, 2\pi)$-uniformly distributed phase θ_j, z_I is, according to the above, a Gaussian random variable whose conditional variance equals

$$\mathrm{var}\,\{z_I \mid \theta_j\} = T_s T_c J_0 \sin^2\theta_j. \tag{100}$$

Hence, the average bit error probability for the I channel when the jammer is present (identically for the Q channel) is given by

$$\begin{aligned}\bar{P}_{b_J}{}^t &= \frac{1}{2\pi}\int_0^{2\pi} Q\left(\sqrt{\frac{ST_s}{2T_cJ_0}}\,\frac{1}{|\sin\theta_j|}\right)d\theta_j \\ &= \frac{2}{\pi}\int_0^{\pi/2} Q\left(\sqrt{\frac{\alpha E_b}{N_J}}\,\frac{1}{\sin\theta_j}\right)d\theta_j\end{aligned} \tag{101}$$

where (18), (94), (97), and (100) have been used and $|\cdot|$ indicates the absolute value. Clearly, the unconditional random variable z_I is not Gaussian, as is also evident from (101).

This last equation can be used in assessing the effect of a spread tone jammer on system performance. However, we shall now indicate an even simpler way of evaluating the tone interference effect by means of converting the spread tone jammer to an *equivalent* AWGN interference, where the equivalence is understood *in terms of its effect on bit error probability*. Let N_{0_J} represent the one-sided power spectral density of AWGN interference whose statistical characteristics remain the same after the PN despreader. Clearly, the bit error probability in this case is given by

$$\bar{P}_{b_J}{}^n = Q\left(\sqrt{\frac{2E_b}{N_{0_J}}}\right). \tag{102}$$

Equations (101) and (102) have been plotted in Fig. 16. The abscissa is the signal-to-jammer power ratio SJR in decibels where, for the spread-tone case $(\mathrm{SJR})^t = \alpha E_b/N_J$ while, for the noise case, $(\mathrm{SJR})^n = E_b/N_{0_J}$.[11] A careful examina-

[9] This also implicitly assumes *contiguous* hop slots within the total band since, if the hop frequency is located in the center of each slot, half of the PN spreading spectrum main lobe will overlap into the two adjacent slots.

[10] Note that having found the conditions for approximating the despread tone as a Gaussian noise does not necessarily guarantee that this approximation will not predict an incorrect "bottoming out" effect. This bottoming out effect occurs at smaller and smaller error probabilities as M gets greater and greater with respect to unity [see [7] for further details].

[11] Note that a "crossover point" exists at about SJR = 0.4 dB, above which the tone jammer is more effective than the noise jammer, while the opposite holds below this crossover point.

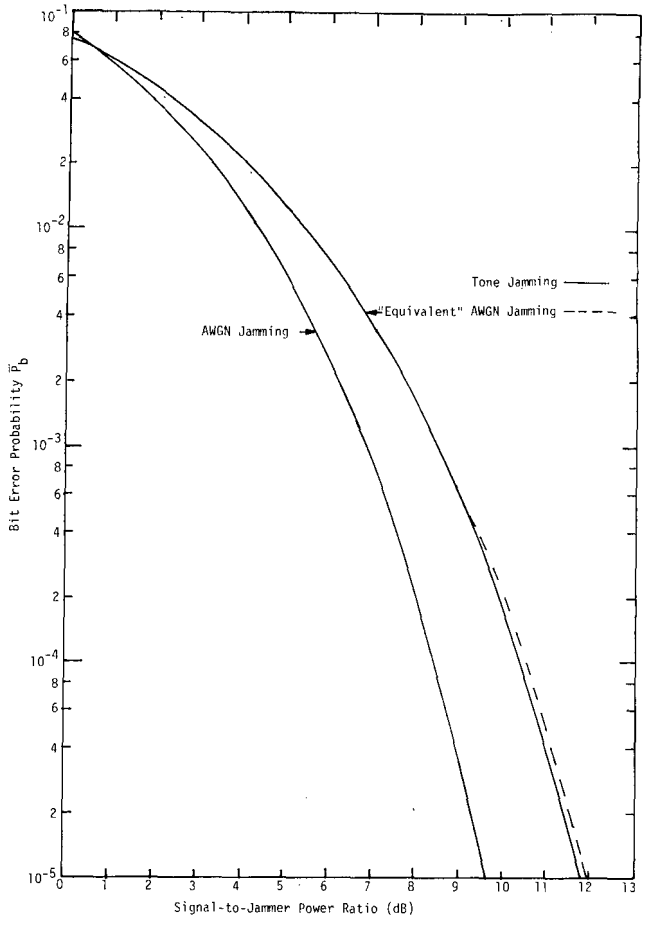

Fig. 16. QPSK bit error probability $\bar{P}_b$ versus SJR (dB) for AWGN and tone jamming and spread-tone "equivalent" AWGN jamming.

tion of Fig. 16 reveals that, for values of $(SJR)^t$ up to approximately 12 dB, the difference $(SJR)^t_{(dB)} - (SJR)^n_{(dB)}$ between the signal-to-jammer ratios which achieve the same performance is, to a high degree of accuracy, linearly increasing with $(SJR)^t_{(dB)}$, the slope of the line being 0.2. It is therefore concluded that, given a spread tone jammer of $(SJR)^t$ dB, an "*equivalent*" AWGN jammer can be devised for which

$$(SJR)_{equiv}{}^n\,(dB) = (0.8) \times (SJR)^t\,(dB). \tag{103}$$

If the SJR's are measured in ordinary numbers rather than decibels, then (103) implies that

$$(SJR)_{equiv}{}^n = ((SJR)^t)^{0.8}. \tag{104}$$

From (102) and (104), it then follows that the spread-tone jammer can be conveniently thought of as an "*equivalent*" AWGN jammer with corresponding bit error probability

$$\bar{P}_{b_J}{}^t = Q\left(\sqrt{2\left(\frac{\alpha E_b}{N_J}\right)^{0.8}}\right). \tag{105}$$

Equation (105) has been plotted in Fig. 16 (dotted lines), from which the high degree of agreement with the exact expression for $\bar{P}_{b_J}{}^t$ can be witnessed.[12] The range of the applicability of (105) is, for the current purposes, more than adequate since, in the frequency bands where the jammer is present, the system is forced to operate at high bit error probabilities (this is especially true when the jammer strategy, i.e., choice of α, has been optimized). From (105), it follows that the overall average bit error probability (accounting for partial-band jamming) is given by[13]

$$\bar{P}_b{}^t = \alpha Q\left(\sqrt{2\left(\frac{\alpha E_b}{N_J}\right)^{0.8}}\right). \tag{106}$$

The worst-case jammer can be found from (106), with algebraic manipulations similar to those in Section IV. The results are[14]

$$\alpha = \frac{0.9220}{E_b/N_J} \tag{107}$$

with corresponding

$$\bar{P}_{b_{max}}{}^t = \frac{0.0789}{E_b/N_J}. \tag{108}$$

A comparison of (108) with (83) indicates that the worst tone jammer is slightly less effective than the worst noise jammer. This is attributed to the fact that after α has been optimized, the "effective" SJR = $\alpha E_b/N_J$ is below the "crossover point" of 0 dB.

VII. PERFORMANCE OF FH/PN-QASK IN THE PRESENCE OF PARTIAL-BAND MULTITONE JAMMING

A line of thought similar to that of Section VI also applies here. The tone/noise jamming equivalence discussed in Section VI is also applicable because the first Q function in (91a) dominates over the other terms in the range of interest. Without belaboring the point, we summarize here the pertinent results (also in the absence of thermal noise):

$$\bar{P}_b{}^t = \alpha \bar{P}_{b_J} \tag{109a}$$

where $\bar{P}_{b_J}$ is given by (90a) with

$$x = \sqrt{2\left(\frac{2\alpha E_b}{5N_J}\right)^{0.8}}. \tag{109b}$$

The corresponding worst-case results are

$$\alpha = \frac{2.3050}{E_b/N_J} \tag{110}$$

[12] Interestingly, the exponent 0.8 also introduces a "crossover point" of the kind discussed in the previous footnote, which is now located at 0 dB, not far from 0.4 dB.

[13] Note that this result assumes the absence of thermal noise.

[14] Comments similar to those in footnote 5 associated with (38) apply to this result.

and

$$\bar{P}_{b_{\max}}{}^{t} = \frac{0.1483}{E_b/N_J}. \tag{111}$$

The argument for the fact that (111) is slightly less than (93) is similar to the one of the previous section.

VIII. CONCLUSIONS

In this paper, we have examined the error probability performance of QPSK and QASK modulations when FH or FH/PN spread spectrum modulation is superimposed to combat the intentional interference introduced by partial-band multitone and noise jammers. For each of the four combined modulation forms, namely, FH-QPSK, FH-QASK, FH/PN-QPSK, and FH/PN-QASK, a worst-case jamming strategy has been determined.

Based on the detailed results derived in the text, the following conclusions can be reached.

- FH-QASK-16 is more susceptible to jamming (noise or multitone) than FH-QPSK (in the limiting case of no background Gaussian noise, the difference in susceptibility is about 2.73 dB).
- Both FH-QPSK and FH-QASK are more susceptible to multitone jamming (in the limiting case of no background Gaussian noise, the difference in susceptibility is about 2 dB for either one).
- For either QPSK or QASK, superimposing a hybrid FH/PN spreading modulation on a multitone jammer converts him to an "equivalent" AWGN jammer (assuming that certain assumptions hold) whose effect can be estimated using (104).

APPENDIX

Consider the Gray code with four transmission levels in one dimension shown in Fig. 17. If such a code is applied to both in-phase and quadrature channels, the resulting modulation scheme is a two-dimensional Gray code for a QASK-16 system. Assuming perfectly coherent demodulating references at the receiver, it follows that the two channels operate independently so that the average bit error probability for QASK-16 equals the bit error probability for each channel.

Let us first evaluate the θ_j-conditional bit error probability for the Q channel assuming that the jammer is present. We start with the following normalized version $z_Q{}'$ of the decision variable z_Q of the Q channel given by (47)

$$z_Q{}' \triangleq \frac{z_Q}{T_s} = b_i\delta + \sqrt{J_0}\cos\theta_j + N_Q{}' \tag{A1}$$

where $N_Q{}' = N_Q/T_s$ and var $\{N_Q{}'\} = N_0/2T_s$. In (A1), the variable b_i takes on the values ± 1, ± 3. If we denote by $\Pr\{k \mid i\}$ the conditional probability

$$\Pr\{k \mid i\} = \Pr\{z_Q{}' \text{ falls in } I_k \mid b_i = i\} \tag{A2}$$

with $k = \pm 1, \pm 3$, $i = 1, 3$, it follows from Fig. 17 and the overall symmetry that the aforementioned conditional probability is given by

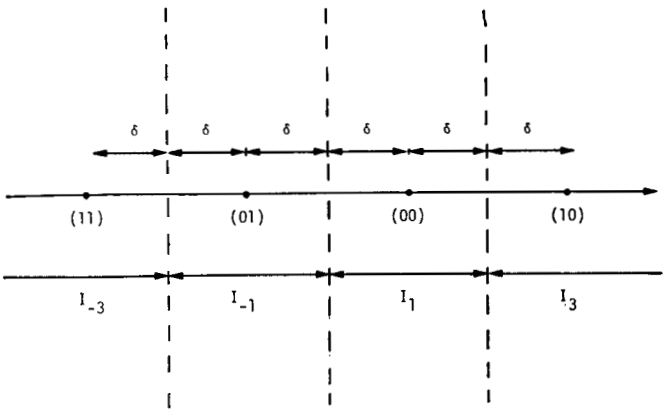

Fig. 17. Gray code for a four transmission-level channel and corresponding decision regions.

$$\bar{P}_{b,Q}(\theta_j) = \tfrac{1}{2}\{\tfrac{1}{2}[\Pr\{3 \mid 1\} + \Pr\{-1 \mid 1\} + 2\Pr\{-3 \mid 1\}] + [\Pr\{1 \mid 3\} + \Pr\{-3 \mid 3\} + 2\Pr\{-1 \mid 3\}]\}. \tag{A3}$$

The outer factor of 1/2 in (A3) accounts for the fact that two bits are transmitted in each Q channel symbol. Equation (A3) can be rewritten as

$$\bar{P}_{b,Q}(\theta_j) = \tfrac{1}{2} - \tfrac{1}{4}[\Pr\{1 \mid 1\} + \Pr\{3 \mid 3\} - \Pr\{-3 \mid 1\} - \Pr\{-1 \mid 3\}]. \tag{A4}$$

But

$$\Pr\{1 \mid 1\} = 1 - Q\left[\sqrt{\frac{2E_b{}'}{N_0}}\left(1 + \sqrt{\frac{N_J}{\alpha E_b{}'}}\cos\theta_j\right)\right] - Q\left[\sqrt{\frac{2E_b{}'}{N_0}}\left(1 - \sqrt{\frac{N_J}{\alpha E_b{}'}}\cos\theta_j\right)\right] \tag{A5}$$

$$\Pr\{3 \mid 3\} = 1 - Q\left[\sqrt{\frac{2E_b{}'}{N_0}}\left(1 + \sqrt{\frac{N_J}{\alpha E_b{}'}}\cos\theta_j\right)\right] \tag{A6}$$

$$\Pr\{-3 \mid 1\} = Q\left[\sqrt{\frac{2E_b{}'}{N_0}}\left(3 + \sqrt{\frac{N_J}{\alpha E_b{}'}}\cos\theta_j\right)\right] \tag{A7}$$

$$\Pr\{-1 \mid 3\} = Q\left[\sqrt{\frac{2E_b{}'}{N_0}}\left(3 + \sqrt{\frac{N_J}{\alpha E_b{}'}}\cos\theta_j\right)\right] - Q\left[\sqrt{\frac{2E_b{}'}{N_0}}\left(5 + \sqrt{\frac{N_J}{\alpha E_b{}'}}\cos\theta_j\right)\right]. \tag{A8}$$

Inserting (A5)–(A8) into (A4) and averaging over θ_j yields the average bit error probability $\bar{P}_{b_J}$ of (67) when the jammer is present. Equation (69) for $\bar{P}_{b_0}$ follows from (67) by eliminating the jammer, i.e., setting $N_J = 0$. Of course, the overall average bit error probability $\bar{P}_b$ is given by (66).

REFERENCES

[1] D. P. Taylor and D. Cheung, "The effect of carrier phase error on the performance of a duobinary shaped QPSK signal," *IEEE Trans. Commun.*, vol. COM-25, pp. 738–744, July 1977.

[2] W. C. Lindsey and M. K. Simon, *Telecommunication Systems Engineering*. Englewood Cliffs, NJ: Prentice-Hall, 1973, ch. 5.

[3] M. K. Simon and J. G. Smith, "Carrier synchronization and detection of QPSK signal sets," *IEEE Trans. Commun.*, vol. COM-22, Feb. 1974.

[4] D. V. Sarwate and M. B. Pursley, "Cross-correlation properties of pseudorandom and related sequences," *Proc. IEEE*, vol. 68, May 1980.

[5] N. E. Bekir, "Bounds on the distribution of partial correlation for PN and Gold sequences," Ph.D. dissertation, Dep. Elec. Eng., Univ. of Southern California, Los Angeles, Jan. 1978.

[6] A. Polydoros and C. L. Weber, "Worst-case considerations for coherent serial acquisition of PN sequences," in *Nat. Telecommun. Conf. Rec.*, Dec. 1980, pp. 24.6.1–24.6.5.

[7] S. Davidovici, D. L. Schilling, and L. B. Milstein, "Analysis of tone interference in DS spread spectrum communications," presented at the 1981 Int. Conf. Commun., Denver, CO, June 1981.

[8] M. K. Simon, "Coherent decision of frequency-hopped quadrature modulations in the presence of jamming—Part II: QPR Class I modulations," this issue, pp. 1661–1668.

Marvin K. Simon (S'60–M'66–SM'75–F'78), for a photograph and biography, see p. 1289 of the September 1981 issue of this TRANSACTIONS.

★

Andreas Polydoros was born in Athens, Greece, in 1954. He received the diploma in electrical engineering from the National Technical University of Athens, Athens, in 1977, and the M.S.E.E. degree from the State University of New York at Buffalo in 1979.

He is currently completing the Ph.D. degree at the University of Southern California, Los Angeles, where he also serves as an Instructor. Since joining Axiomatix, Los Angeles, in 1979, he has worked on a variety of digital communication projects, with emphasis on spread spectrum systems.